LETTERS
https://doi.org/10.1038/s41567-018-0275-9

nature physics

Leidenfrost wheels

Ambre Bouillant[1,2], Timothée Mouterde[1,2], Philippe Bourrianne[1,2], Antoine Lagarde[1,2], Christophe Clanet[1,2] and David Quéré[1,2]*

As reported in 1756 by Johann Gottlob Leidenfrost, volatile liquids on hot solids form "gleaming drops resembling quicksilver", a consequence of their levitation on a vapour cushion[1,2]. This makes the drops spectacularly mobile, moving away as soon as they are deposited—an observation commonly attributed to gravity or surrounding airflows. This mobility has been exploited to manipulate drops, because tiny forces such as those generated on asymmetric substrates can move them in well-defined directions[3-5], a situation that also provides heat evacuation[6]. Here we report that Leidenfrost droplets initially at rest on horizontal substrates self-rotate and self-propel in the direction they are rolling, in the absence of any source of asymmetry or external force. Their rapid internal flow is found to be accompanied by a tilting of their base, which creates a permanent ratchet-like mechanism, entraining the rolling liquid despite the fact that it is not in contact with its substrate.

Levitation occurs when solids sustaining volatile liquids are brought above the so-called Leidenfrost temperature T_L, at which vapour separates the liquid from its substrate[7]. The T_L is about 200 °C for water on a flat solid and it can vary markedly for rough surfaces[8–11]. Above the T_L, drops levitate above a vapour cushion with a typical thickness of 50 μm (refs [12–14]), which makes them highly mobile: studying the Leidenfrost phenomenon requires the immobilization of liquids, using gravitational wells[2] and other traps[15], or simply by contacting them with a needle[12]. Without contact with their hot substrate, drops are observed to slowly evaporate (no boiling) in a fully non-wetting state. Denoting ρ and γ as the liquid density and surface tension, and g as the acceleration due to gravity, drops smaller than the capillary length $\kappa^{-1} = (\gamma/\rho g)^{1/2}$ are quasi-spherical[16,17], while large puddles are flattened with a height $h = 2\kappa^{-1}$, that is, 5.0 mm for water at 100 °C (ref. [12]). In the latter case, gravity also induces beneath the liquid a vapour blister with thickness increasing with the puddle size[16–19] and eventually forming a chimney[12,17–19].

Despite its generality, the elementary situation of free drops placed at rest on flat, horizontal, hot solids has not been considered so far. To that end, we simply dispense water (containing tracers) from a needle (Fig. 1a), as done in classical wetting studies. The needle is located at a distance $H < 2\kappa^{-1}$ above the substrate whose horizontality is adjusted with a highly sensitive spirit level (precision $\alpha_o \approx 0.1$ mrad). Water gently evaporates and detaches from the needle when its equatorial diameter $2R$ is comparable to H. Remarkably, all millimetre-size droplets are observed to rotate as wheels and to spontaneously propel in the wheel direction after detachment (Supplementary Video 1). Figure 1b shows a liberated water drop gradually fleeing away and becoming blurry as it escapes the half-millimetric field depth of the camera. Top views can be also performed and we show in Fig. 1c the trajectories of 100 drops with radius $R \approx 1$ mm and mass $m \approx 4$ mg initially at the centre of a silicon wafer at $T = 350$ °C. Distinctive colours are used for successive paths, which highlights that all drops escape from their initial location following straight lines and random directions (Supplementary Video 2). The time $\tau \approx 1$–3 s at which they leave the wafer is much shorter

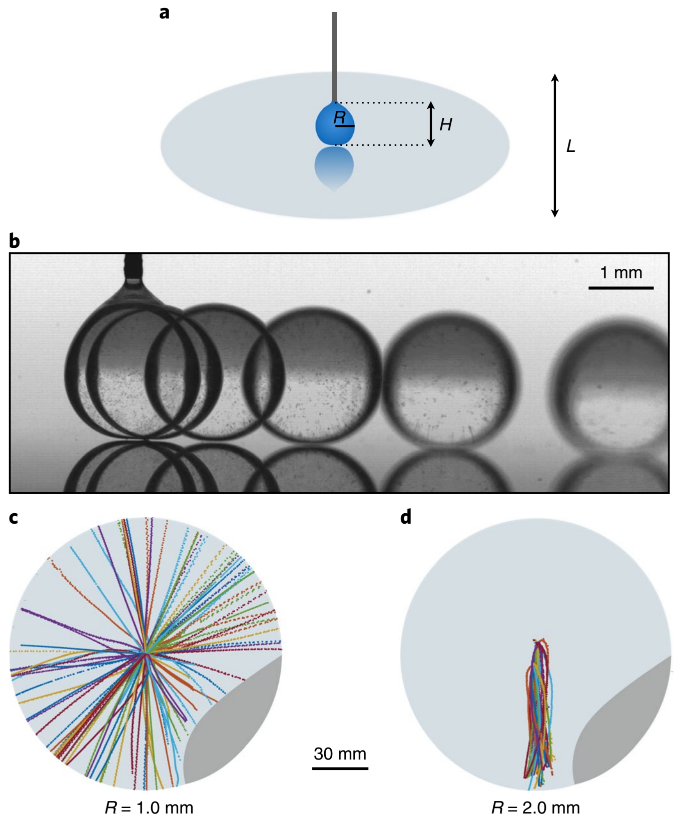

Fig. 1 | Behaviour of Leidenfrost drops starting from rest on flat silicon wafers. a, Schematic of the experiment: a quasi-spherical water drop with radius R sits at the centre of a hot wafer with diameter L. Water containing tracers is dispensed from a needle located at a millimetre-size distance H above the substrate. Owing to evaporation, it detaches at a radius $R \approx H/2$. **b**, Chronophotography (timestep of 94 ms) of a water drop with radius $R = 1.10$ mm. Once liberated, the Leidenfrost drop self-propels on the reflective wafer heated at $T = 300$ °C (see also Supplementary Video 1). **c**, Superimposition of 100 trajectories (top views, $R = 1.00 \pm 0.05$ mm) on a wafer at $T = 350$ °C. All drops self-propel after detachment with straight, isotropic trajectories (Supplementary Video 2). The grey zone on the bottom right is hidden by the needle and thus inaccessible experimentally. **d**, Same experiment for 40 drops with radius $R = 2$ mm. The roughly straight-line trajectories now follow a common direction (Supplementary Video 2).

[1]Physique et Mécanique des Milieux Hétérogènes, UMR 7636 du CNRS ESPCI, PSL Research University, Paris, France. [2]LadHyX, UMR 7646 du CNRS, École Polytechnique, Palaiseau, France. *e-mail: david.quere@espci.fr

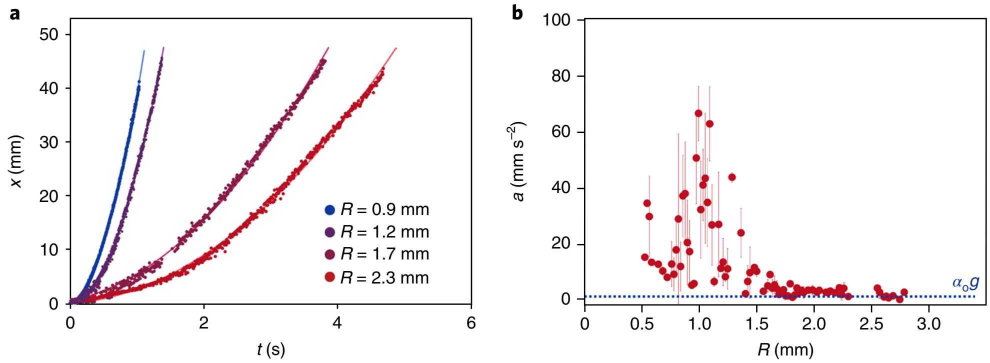

Fig. 2 | Dynamics of self-propelled Leidenfrost drops. a, Position x of the drop as a function of time t, for four drops (with different radius) placed on the same wafer heated at $T = 350\,°C$. Each curve is fitted by a quadratic function (drawn with a solid line), from which we deduce the acceleration a. **b**, Acceleration a as a function of the equatorial radius R for 270 experiments. Drops with $R > 1.5$ mm are in the biased regime (Fig. 1d) where a is comparable to $\alpha_o g$ (dotted line), the gravitational acceleration defined with our precision α_o on horizontality. For $R < 1.5$ mm, a critically increases and becomes non-monotonic in R. This regime corresponds to the isotropic trajectories of Fig. 1c, and error bars show the standard dispersion of the data.

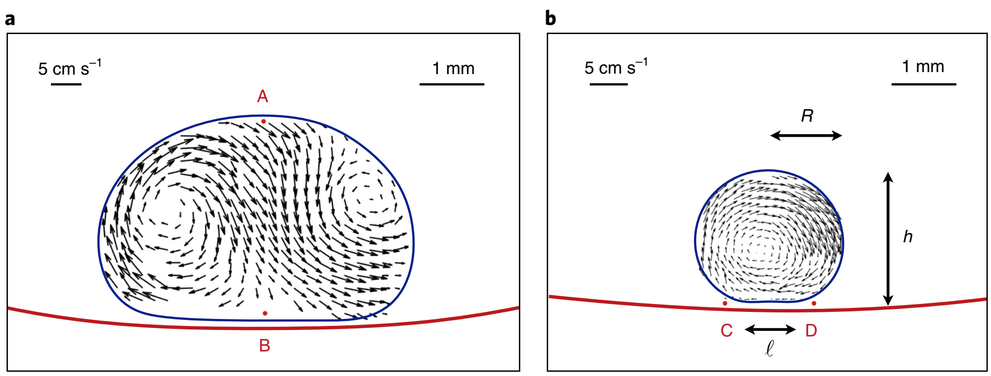

Fig. 3 | Influence of the drop shape on its inner dynamics. PIV measurements are performed in the central plane of a water drop immobilized on a slightly curved solid (indicated in red) heated at $T = 300\,°C$. Bars show a velocity scale of $5\,cm\,s^{-1}$ and a spatial scale of 1 mm and blue lines stress the drop contours. **a**, For a gravity-flattened drop ($R = 2.45 \pm 0.05$ mm), tracers reveal the existence of two internal convective cells in the illuminated slice flowing along the interface from the base B to the apex A (see also Supplementary Video 3). Image is slightly distorted by curvature but the distortion does not change the morphology of inner motions[31]. **b**, For a quasi-spherical drop ($R = 1.15 \pm 0.05$ mm), the flow symmetry is broken and we observe a simple rolling motion (Supplementary Video 4). Air entrained by the flow enters the vapour film at point D and exits at point C.

than the evaporation time (a few minutes), so that we can neglect the variation of their radius R.

Hence Leidenfrost droplets propel without external forces or roughness, and their directional motions demonstrate that these drops are not only ultra-mobile[20] but also able to generate and sustain their own dynamics. Observations differ for larger drops, as seen in the 40 trajectories of Fig. 1d for $R = 2$ mm. They now follow a unique direction, as expected for non-adhesive liquids in the gravity field. The precision on horizontality being $\alpha_o \approx 0.1$ mrad, frictionless drops will cross the wafer (of diameter $L = 10$ cm) in $\tau \approx (L/g\alpha_o)^{1/2} \approx 10$ s, as observed here. In contrast, the fast, isotropic motions reported in Fig. 1b,c reveal a self-propelling force much larger than $mg\alpha_o$, which we now investigate.

As seen in Fig. 2a, the position $x(t)$ of the drop centre in both self-propelling ($R \approx 1$ mm) and biased regimes ($R \approx 2$ mm) is convincingly fitted by parabolas (solid lines), which provides the drop acceleration a. As shown in Fig. 2b, a critically depends on R. For $R > 1.5$ mm (biased trajectories), it is a few $mm\,s^{-2}$, that is, comparable to the residual gravitational acceleration $\alpha_o g \approx 1\,mm\,s^{-2}$ indicated with a dotted line in the figure. For $R < 1.5$ mm, acceleration is much larger, more scattered and non-monotonic with R. Each data point corresponds to ten independent experiments, as commented in the Supplementary Information (Supplementary Fig. 2). The acceleration is typically $40\,mm\,s^{-2}$ and it can even reach $87\,mm\,s^{-2}$ for $R \approx 1.2$ mm (Supplementary Fig. 2a), values about 50 times larger than $\alpha_o g$.

As shown in the Supplementary Fig. 3, all observations are found to resist a variation of substrate temperature from 250 °C to 450 °C. Self-propulsion can even be observed down to 150 °C (Supplementary Fig. 5) when using super-hydrophobic materials with a lower Leidenfrost point[11]. The robustness of the effect can also be tested by considering substrates that are rough at scales between micrometres and tens of micrometres. As seen in Supplementary Figs. 4–6, isotropic self-propulsion remains unchanged, provided the substrate is hot enough to enable levitation.

Self-propulsion emerges when drops are quasi-spherical, in a regime where gravity only flattens the liquid base by a distance $\ell \approx R^2\kappa < R$ (Fig. 3b and Supplementary Fig. 7)[21]. As shown in Fig. 3 and in Supplementary Videos 3 and 4, the drop shape impacts the internal flow, as demonstrated by particle image velocimetry (PIV). For drops larger than 1.5 mm (Fig. 3a), this flow consists of counter-rotative convective cells (in the plane of illumination) with a surface velocity of ~$5\,cm\,s^{-1}$. With such symmetric flows, we do not expect (nor report) self-propulsion. In contrast, quasi-spherical drops exhibit a unique rotating cell (Fig. 3b), before self-propelling in the direction of rotation after detachment from the needle. Remarkably,

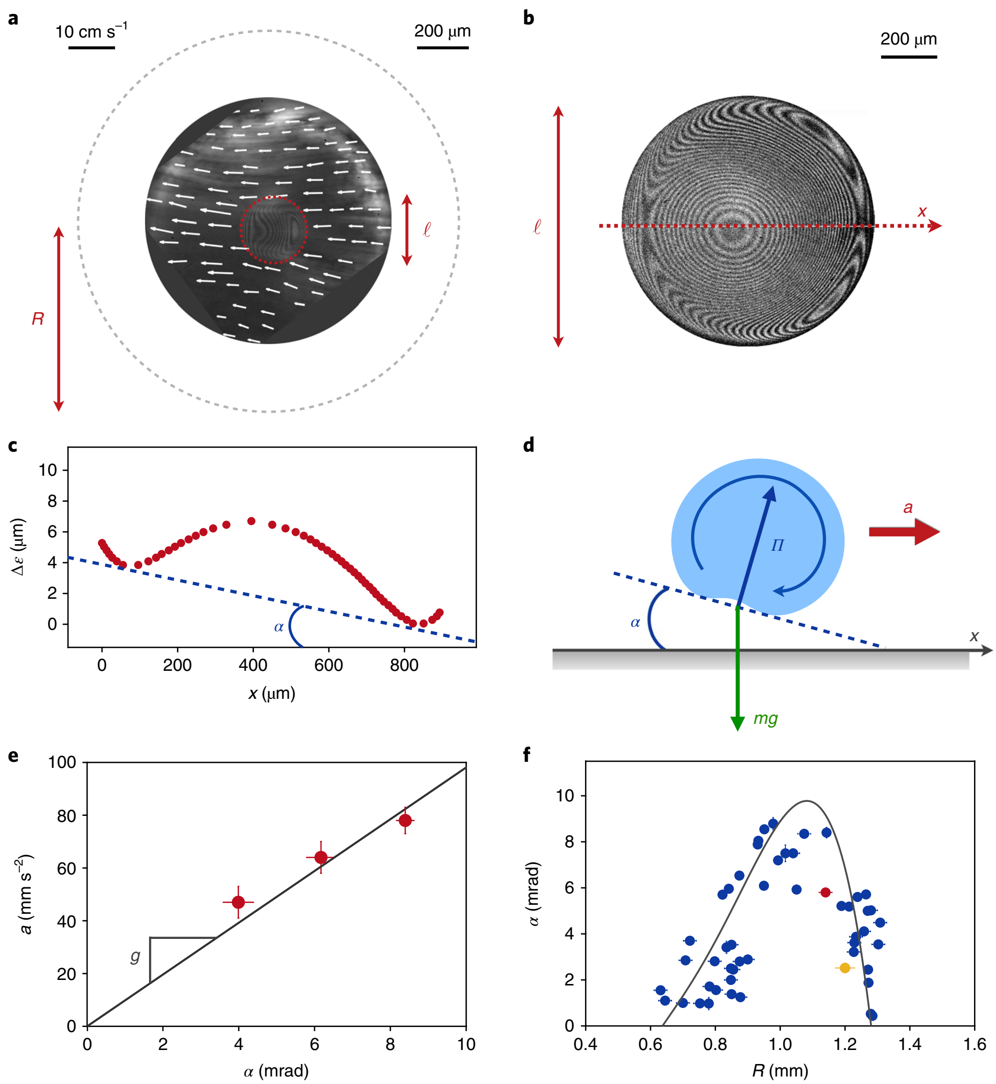

Fig. 4 | Focus on the base of self-propelling drops. a, Simultaneous PIV and interferometric visualization of the bottom of a Leidenfrost droplet ($R = 0.73$ mm, indicated with a dashed line) immobilized by a needle on a hot transparent sapphire ($T = 300$ °C). Tracers near the surface move along the symmetry axis of the interference pattern at a velocity V of a few cm s^{-1}. **b**, Interference pattern in the contact zone (size $l \approx 800$ μm) for a drop with radius $R = 1.15$ mm. Focus and illumination are the same as in **a**. The vapour profile beneath the drop is observed to be asymmetric as evidenced by the off-centering of the vapour blister. **c**, Liquid/vapour interface relative thickness $\Delta\varepsilon$ along the x axis defined in **b** in the interference pattern. The drop base is tilted on average by an angle $\alpha \approx 3$ mrad. Error bars on the thickness correspond to the fringe width and are typically 0.1 μm. **d**, Drop (mass m) levitating above a cushion of vapour tilted by a small angle α and thus subjected to a horizontal force $\Pi\alpha = mg\alpha$ and to an acceleration $a = \alpha g$. **e**, Simultaneous measurements of drop acceleration a and tilt α, using two synchronized cameras: one offering a side view (leading to a), the other capturing interferences (leading to α). The solid line shows the slope g and errors bars correspond to the standard deviation of the data. **f**, Tilt angle α for drops immobilized by a needle just before detachment as a function of their radius R. A peak in tilt is observed between 0.7 and 1.3 mm, that is, in the exact range of self-propulsion. The solid line is a guide for the eyes. Two supplementary data extracted from photos by Burton et al.[16] and by Pomeau et al.[17] are shown in yellow and red, respectively.

Leidenfrost himself reported "a very swift motion of turning, which is seen when a small coloured speck, for example, some black carbon, adheres to the drop"[2].

Despite this early observation, these motions and their origin have been hardly discussed in the literature. They can stem from the vapour flow in the subjacent film. This viscous flow of typical velocity $U \approx 10$ cm s^{-1} (ref. [12]) entrains water from the base centre (point B in Fig. 3a) to the periphery, which generates circulation to the apex (point A) and downward along the symmetry axis (AB). The typical velocity V of this flow is deduced from the continuity of viscous stress, $\eta V/R \sim \eta_v U/\varepsilon$, where η_v and ε are the vapour viscosity and thickness, respectively, and η is the water viscosity. For $\eta_v \approx 16\,\mu$Pa s (at 200 °C), $\eta \approx 0.3$ mPa s (taken at the boiling point), $R = 1$ mm and $\varepsilon \approx 100$ μm, V is expected to be a fraction of U, that is, a few cm s^{-1}, in agreement with Fig. 3 ($V \approx 5$ cm s^{-1}).

Motion may also be temperature driven. Liquid temperature is maximum at the bottom (point B, close to the plate) and at the core (far from interfaces). The temperature difference ΔT within the drop is a few degrees, as shown in Supplementary Figs. 8 and S9) and in ref. [22]. Such inhomogeneity has two consequences. (1) The decrease of surface tension with temperature ($|d\gamma/dT| \approx 0.1$ mN m^{-1} K^{-1}) generates interfacial Marangoni flows from hot to cold[20,23], that is, from B to A following interfaces, in accord with Fig. 3a. At Reynolds numbers $\rho RV/\eta$ of typically 500, the Marangoni force $(d\gamma/dT)\Delta TR$ is resisted by inertia, of order ρV^2R^2. Hence we get: $V \sim (|d\gamma/dT|\Delta T/\rho R)^{1/2} \approx 3\,\mathrm{cm\,s^{-1}}$, a velocity comparable to that induced by vapour. However, infrared observations show that temperature homogenizes with rolling motion (Supplementary Fig. 9), suggesting that vapour effects are dominant in this regime. (2) Temperature differences also generate a buoyancy-driven rise with a downward interfacial recirculation, in contradiction to Fig. 3a. For an expansion coefficient of water $\alpha_T \approx 0.7\,\mathrm{mK^{-1}}$, the force balance $\rho g\alpha_T\Delta TR^3 \approx \rho V^2R^2$ yields $V \sim (g\alpha_T\Delta TR)^{1/2} \approx 5\,\mathrm{mm\,s^{-1}}$, a speed much smaller than observed, which confirms the marginal role of this effect.

The flow geometry finally depends on the drop aspect ratio. When $2R/h$ is significantly larger than unity (puddles), the inner flow forms several symmetric cells in the plane of observation (Fig. 3a). However, this is not anymore permitted as $2R/h$ becomes of order unity ($\kappa R < 0.6$, Fig. 3b): as known for Rayleigh–Bénard instabilities[24], confinement induces symmetry breaking when the liquid cell can only host a unique roll (Fig. 3b and Supplementary Video 5). For drops slowly evaporating on hydrophobic substrates, flow patterns similarly switch from symmetric to asymmetric as the aspect ratio changes from a value of order 2 to a value of order 1—even if motions are then roughly 100 times slower than here[25,26].

Symmetry breaking alone does not explain propulsion: water levitates, which impedes a direct conversion of rotation into translation. For instance, drops levitating on hydraulic jumps rotate but get entrained along the hydraulic flow, that is, opposite to the rotation direction[27]. On immobile substrates, the vapour entrained by the rotating liquid produces a viscous drag in the direction opposed to propulsion. This force scales as $(\eta_v V/\varepsilon)\ell^2$, a quantity below $0.01\,\mu\mathrm{N}$, at least one order of magnitude smaller than measured. To understand how the internal flow impacts the vapour film, we performed interferometric measurements, using a high-speed camera mounted on an inverted microscope[18,19]. We immobilize a water drop on a hot transparent sapphire ($T = 300\,°\mathrm{C}$) and overlap successive images of the lower hemisphere. As seen in Fig. 4a (and Supplementary Video 6), tracers follow a path aligned with the symmetry axis of the interference pattern and travel at a speed V of a few $\mathrm{cm\,s^{-1}}$, in agreement with the data in Fig. 3 (see also Supplementary Fig. 10). Keeping the same illumination and focus, we look closer at the interferences at the drop base, which provides key observations. As seen in Fig. 4b, the vapour blister evidenced by fringes is off-centred, a first hint of an asymmetry in the vapour profile. The variation $\Delta\varepsilon$ of vapour thickness in Fig. 4c first confirms the modest height ($\sim 5\,\mu\mathrm{m}$) of blisters beneath millimetre-size drops, compared with their width $\ell \approx 1.6R^2\kappa \approx 800\,\mu\mathrm{m}$; but more importantly, the bottom interface appears to be tilted by an angle α ($\alpha \approx 2.9 \pm 0.5\,\mathrm{mrad}$ here), which we interpret as a consequence of rotation. The drop entrains an air layer of typical speed V, the velocity inside the liquid. This airflow perturbs the evacuation of vapour to make its speed smaller at the 'entrance' of the gap (point D in Fig. 3b) than at the 'exit' (point C). The vapour flow being viscous, we expect a pressure difference $\Delta p = p_C - p_D$ scaling as $\eta_v V\ell/\varepsilon^2$, which lifts the exit region. The amplitude $\Delta\varepsilon$ of the lift is obtained by balancing Δp with the Laplace pressure (dominant at this scale) $\gamma\Delta\varepsilon/\ell^2$. We get $\alpha \approx \Delta\varepsilon/\ell \approx \eta_v V\ell^2/\gamma\varepsilon^2$, that is, 1–10 mrad for the parameters of our experiment, in agreement with the data in Fig. 4. This value is expected to be stationary, as confirmed in Supplementary Fig. 10).

A tilt of the drop base will induce propulsion (Fig. 4d). The levitating pressure force Π balancing the drop weight mg then has a horizontal component $\Pi\alpha \approx mg\alpha$, which accelerates water along the x axis defined in Fig. 4b by $a \approx \alpha g$ (ref. [5]). A direct check of this formula is not easy: drops being isotropically propelled (Fig. 1c), simultaneous side and bottom observations are difficult to perform. However, we succeeded in making three synchronized views from below (which yields α) and from the side (which yields a), and Fig. 4e shows a quantitative agreement with the prediction, without any adjustable parameter. The small value of α might explain the dispersion of the data in Fig. 2b: drops slightly oscillate as they move (Supplementary Video 7), which can perturb the vapour thickness and thus the measured acceleration.

Our scenario implies that the tilt α depends on R. At large R, internal flows become symmetric (Fig. 3a), which should make α vanish. At small R, we also expect a decrease of propulsion since inner flows then get weaker: drops whose base width ℓ varies as R^2 become quasi-spherical, which geometrically quenches vapour and liquid flows (see also Supplementary Fig. S9). Measurements in Fig. 4f indeed exhibit a non-monotonic behaviour for $\alpha(R)$. Data form a well-defined peak between 0.7 and 1.3 mm, in the exact range of self-propulsion: αg matches the peak in acceleration reported in Fig. 2b, both in amplitude and width.

The elusive character of drops on hot plates is routinely attributed to levitation, making them sensitive to any force (weak tilt, airflows). We reported here that millimetre-size droplets propel without external field, which contributes to, and even explains, their legendary mobility. Self-propulsion arises from an asymmetry in the vapour profile, as though droplets were transporting their own, stationary ratchet. It would be interesting to look at the behaviour of these drops as they hit (hot) walls or other drops. Conversely, our findings might allow us to design new kinds of self-propelling devices: a Leidenfrost liquid on a solid with a temperature gradient might spontaneously move to the cold[28], owing to the dependency of the vapour thickness on temperature—showing again that the conjunction of phase change with frictionless motion generates a rich landscape of novel situations. Our scenario might finally help to understand propulsion in other levitating states, such as observed for drops sitting on vibrating baths[29]. For special amplitude and frequency, these levitating drops were found to both rotate and oscillate non-axisymmetrically, which is accompanied by a (slow, compared with our case) translation[30]—an observation that remains to be understood.

Online content

Any methods, additional references, Nature Research reporting summaries, source data, statements of data availability and associated accession codes are available at https://doi.org/10.1038/s41567-018-0275-9.

Received: 2 March 2018; Accepted: 9 August 2018;
Published online: 10 September 2018

References

1. Boerhaave, H. *Elementae Chemiae* Vol. 1 (Lugduni Batavorum, Leiden, 1732).
2. Leidenfrost, J. G. *De Aquae Communis Nonnullis Qualitatibus Tractatus* (Ovenius, Duisburg, 1756); transl. Wares, C. On the fixation of water in diverse fire. *Int. J. Heat Mass Trans.* **9**, 1153–1166 (1966).
3. Linke, H. et al. Self-propelled Leidenfrost droplets. *Phys. Rev. Lett.* **96**, 154502 (2006).
4. Marín, A. G. et al. Capillary droplets on Leidenfrost micro-ratchets. *Phys. Fluids* **24**, 1–9 (2012).
5. Dupeux, G. et al. Self-propelling uneven Leidenfrost solids. *Phys. Fluids* **25**, 051704 (2013).
6. Singh Dhillon, N., Buongiorno, J. & Varanasi, K. K. Critical heat flux maxima during boiling crisis on textured surfaces. *Nat. Commun.* **6**, 8247 (2015).
7. Bernardin, J. D. & Mudawar, I. The Leidenfrost point: experimental study and assessment of existing models. *J. Heat Transf.* **121**, 894–903 (1999).
8. Bernardin, J. D. & Mudawar, I. Film boiling heat transfer of droplet streams and sprays. *Int. J. Heat Mass Transf.* **40**, 2579–2593 (1997).
9. Weickgenannt, C. M. et al. Inverse-Leidenfrost phenomenon on nanofiber mats on hot surfaces. *Phys. Rev. E* **84**, 036310 (2011).
10. Arnaldo del Cerro, D. et al. Leidenfrost point reduction on micropatterned metallic surfaces. *Langmuir* **28**, 15106–15110 (2012).
11. Vakarelski, I. U., Patankar, N. A., Marston, J. O., Chan, D. Y. C. & Thoroddsen, S. T. Stabilization of Leidenfrost vapour layer by textured superhydrophobic surfaces. *Nature* **489**, 274–277 (2012).
12. Biance, A. L., Clanet, C. & Quéré, D. Leidenfrost drops. *Phys. Fluids* **15**, 1632–1637 (2003).

13. Gottfried, B. S., Lee, C. J. & Bell, K. J. The Leidenfrost phenomenon: film boiling of liquid droplets on a flat plate. *Int. J. Heat Mass Trans.* **9**, 1167–1188 (1966).
14. Myers, T. G. & Charpin, J. P. F. A mathematical model of the Leidenfrost effect on an axisymmetric droplet. *Phys. Fluids* **21**, 63101–1632 (2009).
15. Cousins, T. R., Goldstein, R. E., Jaworski, J. W. & Pesci, A. I. A ratchet trap for Leidenfrost drops. *J. Fluid Mech.* **696**, 215–227 (2012).
16. Burton, J. C., Sharpe, A. L., Van der Veen, R. C. A., Franco, A. & Nagel, S. R. Geometry of the vapor layer under a Leidenfrost drop. *Phys. Rev. Lett.* **109**, 074301 (2012).
17. Pomeau, Y., Le Berre, M., Celestini, F. & Frisch, T. The Leidenfrost effect: from quasi-spherical droplets to puddles. *C. R. Mec.* **340**, 867–881 (2012).
18. Duchemin, L., Lister, J. R. & Lange, U. Static shapes of levitated viscous drops. *J. Fluid Mech.* **533**, 161–170 (2005).
19. Snoeijer, J. H., Brunet, P. & Eggers, J. Maximum size of drops levitated by an air cushion. *Phys. Rev. E* **79**, 036307 (2009).
20. Quéré, D. Leidenfrost dynamics. *Annu. Rev. Fluid Mech.* **45**, 197–215 (2013).
21. Mahadevan, L. & Pomeau, Y. Rolling droplets. *Phys. Fluids* **11**, 2449–2453 (1999).
22. Wciślik, S. Thermal infrared mapping of the Leidenfrost drop evaporation. *J. Phys. Conf. Ser.* **745**, 32064 (2016).
23. Mrinal, M., Wang, X. & Luo, C. Self-rotation induced propulsion of a Leidenfrost drop on a ratchet. *Langmuir* **33**, 6307–6313 (2017).
24. Touihri, R., Ben Hadid, H. & Henry, D. On the onset of convective instabilities in cylindrical cavities heated from below. I. Pure thermal case. *Phys. Fluids* **11**, 2078–2088 (1999).
25. Tam, D., von Arnim, V., McKinley, G. H. & Hosoi, A. E. Marangoni convection in droplets on superhydrophobic surfaces. *J. Fluid Mech.* **624**, 101–123 (2009).
26. Dash, S., Chandramohan, A., Weibel, J. A. & Garimella, S. V. Buoyancy-induced on-the-spot mixing in droplets evaporating on nonwetting surfaces. *Phys. Rev. E* **90**, 062407 (2014).
27. Duchesne, A., Savaro, C., Lebon, L., Pirat, C. & Limat, L. Multiple rotations of a drop rolling inside a horizontal circular hydraulic jump. *Eur. Phys. Lett.* **102**, 64001 (2013).
28. Sobac, B., Rednikov, A., Dorbolo, S. & Colinet, P. Self-propelled Leidenfrost drops on a thermal gradient: a theoretical study. *Phys. Fluids* **29**, 082101 (2017).
29. Couder, Y., Fort, E., Gautier, C. H. & Boudaoud, A. From bouncing to floating: noncoalescence of drops on a fluid bath. *Phys. Rev. Lett.* **94**, 177801 (2005).
30. Dorbolo, S., Terwagne, D., Vandewalle, N. & Gilet, T. Resonant and rolling droplet. *New J. Phys.* **10**, 113021 (2008).
31. Kang, K. H., Lee, S. J., Lee, C. M. & Kang, I. S. Quantitative visualization of flow inside an evaporating droplet using the ray tracing method. *Meas. Sci. Technol.* **15**, 1104–1112 (2004).

Acknowledgements

We thank C. Frot for her help in designing the set-up, J. Quintela Casal for preliminary experiments and C. Josserand and É. Pirot for fruitful discussions.

Author contributions

T.M., P.B., C.C. and D.Q. conceived the project. A.B., T.M., P.B. and D.Q. designed the project. A.B. performed most experiments and analyses to which A.L. also contributed. A.B., T.M., C.C. and D.Q. discussed the models. A.B. and D.Q. wrote the manuscript with inputs from all other authors.

Competing interests

The authors declare no competing interests.

Additional information

Supplementary information is available for this paper at https://doi.org/10.1038/s41567-018-0275-9.

Reprints and permissions information is available at www.nature.com/reprints.

Correspondence and requests for materials should be addressed to D.Q.

Publisher's note: Springer Nature remains neutral with regard to jurisdictional claims in published maps and institutional affiliations.

Methods

The different techniques for visualizing drops, inner flows and vapour gaps are as follows. (1) For global measurements (Figs. 1 and 2), drops can be simultaneously tracked from the side and from the top, using high-speed cameras (Phantom V9) filming at 50 to 4,000 frames per second. Trajectories deduced from top views are found to be fitted by quadratic functions $x = a(t - t_o)^2/2$ (coloured lines in Fig. 2a), where the adjusted departure time $t_o \approx 10$ ms is always much smaller than the travel duration $\tau \approx 1$–10 s, and comparable to the oscillation time at detachment. (2) Internal flows are obtained from PIV. Tracers (hollow glass spheres Sphericel 110P8 with a diameter of 11.7 μm and a density of 1,100 kg m^{-3}) are dispersed in water and drops are immobilized either by the dispensing needle or by a slight curvature at the solid surface (results are independent of the technique of immobilization). Illumination is provided by a 400-μm-thick sheet originating from a He-Ne laser (wavelength $\lambda = 633$ nm), and a high-speed camera focusing on the illuminated slice takes pictures at 1,000 to 4,000 frames per second. We deduce the local velocity from successive images (time step: 1 ms), as reported in Fig. 3.
(3) Interferometric measurements in Fig. 4 are performed with a high-speed camera mounted on an inverted microscope. Water is immobilized with a needle on a hot transparent sapphire brought to $T = 300$ °C and ten successive images of the lower hemisphere shot at 500 frames per second are overlapped (Fig. 4a) while the interference pattern at the drop base is recorded (Fig. 4b).

Data availability

The data that support the plots within this paper and other findings of this study are available from the corresponding author upon request.